CHEMISTRY
AN ASIAN JOURNAL
www.chemasianj.org

Accepted Article

Title: A novel activatable and switchable nanoaggregate probe for detecting H2S and its application in mice brains

Authors: Ya-Lin Qi, Li-Li Chen, Long Guo, Yu-Shun Yang, Zhen-Xiang He, and Hai-Liang Zhu

To be cited as: *Chem. Asian J.* 10.1002/asia.202000964

Link to VoR: https://doi.org/10.1002/asia.202000964

A Journal of
ACES Asian Chemical Editorial Society

A sister journal of Angewandte Chemie and Chemistry – A European Journal

WILEY-VCH

10.1002/asia.202000964

A novel activatable and switchable nanoaggregate probe for detecting H_2S and its application in mice brains

Ya-Lin Qi, [#] Li-Li Chen, [#] Long Guo, Chen-Wen Shao, Ya-Ni Liu, Yu-Shun Yang,[*] Zhen-Xiang He,[*] and Hai-Liang Zhu[*]

State Key Laboratory of Pharmaceutical Biotechnology, School of Life Sciences, Nanjing University, Nanjing, 210023, China.

E-mail: zhuhal@nju.edu.cn; ys_yang@nju.edu.cn; zxhe@nju.edu.cn.

[#] Both authors contributed equally to this work.

Abstract: Employing a sequentially activated probe design method, an activatable, switchable and dual-mode probe was designed. This nanoprobe, **HSDPP**, could be effectively activated by H_2S to form H-type aggregates with green emission; subsequently, the aggregates could bind to mtDNA to form monomers and the emssion color switched from green to deep-red. We exploited **HSDPP** to image the exogenous and endogenous H_2S in living cells. Of note, for the first time, this novel nanoprobe with an optimal partition coefficient value (LogP = 1.269) was successfully applying for tracking the endogenous H_2S upregulation stimulated by cystathionase activator *S*-adenosyl-*L*-methionine (SAM) in mice brains. Finally, our work provides an invaluable chemical tool for probing endogenous H_2S upregulation *in vitro/vivo* and, importantly, affords a prospective design strategy for developing switchable chemosensors to unveil the relationship between the biomolecules and DNA in mitochondrial in many promising areas.

Introduction

Molecular probes, which have been widely utilized to track biomarkers and molecular events in living biosystems, can be broadly categorized into two fields including “always on” tags and activatable sensors.[1] “Always on” tags produce contrast signals through accumulation and, particularly, their signals keep stable within the position or situation of interest.[2] On the contrary, serving as molecular beacons or optical switches, activatable probes are commonly in the “off” state at the beginning and can only be stimulated by the certain target to send out corresponding signals.[3,4] In comparison with the nonresponsive species ("always off") and the "always on" tags, the activatable probes benefit from the signal changes, which further lead to the

advantages including higher signal-to-noise ratio, lower detection of limit, permitting sensitive and so on.[5–7] Therefore, they are capable of responding specifically to the biomarkers of diseases and allow disease-specific diagnosis.[8] Accordingly, investigators have paid an increasing attention to the activatable probes in recent years.[9–12]

On the other hand, as the third multifunctional gasotransmitter, H_2S has been recognized as an important signaling molecule in the cardiovascular and nervous systems.[13,14] There is not much to debate anymore about the significance on monitoring the internal level of H_2S,[15–18] however, when the investigations nowadays come to the tissues or models *in vivo*, near-infrared (NIR) implements seem more favoured due to the strong penetrability and photothermal/photoacoustic effect.[19] No matter the probes are small molecular or nanoscale ones,[20,21] one major concern is maintaining obvious reporting signals to guarantee both sensitivity and selectivity. Basically, longer wavelength means weaker energy, thus a direct NIR sensing usually need a subsequent procedure of amplification. Common enlarging strategies include instrumental calibration,[22] Aggregation-Induced Emission (AIE),[23,24] protein-assistant amplification,[25,26] nanocarrier-based signal transmission,[27] and so on. One step further, we still hope that the signal switching could be regulated by an "all-or-nothing" biomolecule which itself is the marker of specific physiological or pathological models, for example, glutathione in solid tumor [28] or caspase-3 in apoptosis.[29] For the monitoring of H_2S, the requirements become specialized because the internal H_2S is usually at the micromole level.[30] Thus, in spite of the high sensitivity, the major concern is introducing stable NIR signals under a model-specific regulation. Accordingly, we put our attention on Mitochondrial DNA (mtDNA).[31] As a significant biomarker in bioenergetics and biochemistry, mtDNA shows at least two favourable features for acting as the signal switcher. One is that mtDNA is ubiquitously existing in eukaryotic cells with a certain level.[32] The other is that mtDNA is associated with several inherited diseases, including inflammation, autoimmunity, and aging.[33–36] Among these diseases, the mtDNA level is remarkably affected in specific positions such as brain and heart, while these positions are also the key ones for H_2S-associated diagnose.[37–39] Although a variety of small molecular fluorescent probes have been reported for detecting H_2S or mtDNA independently,[40–43] in

10.1002/asia.202000964

this work, we attempted to combine them into a detecting system which was activatable, switchable and available for applications in brains.

Herein, we exploited a novel activatable and switchable probe, **HSDPP**, for monitoring the H_2S level *in vitro* and *in vivo* with two different channels (Scheme 1). Consulting the recognition

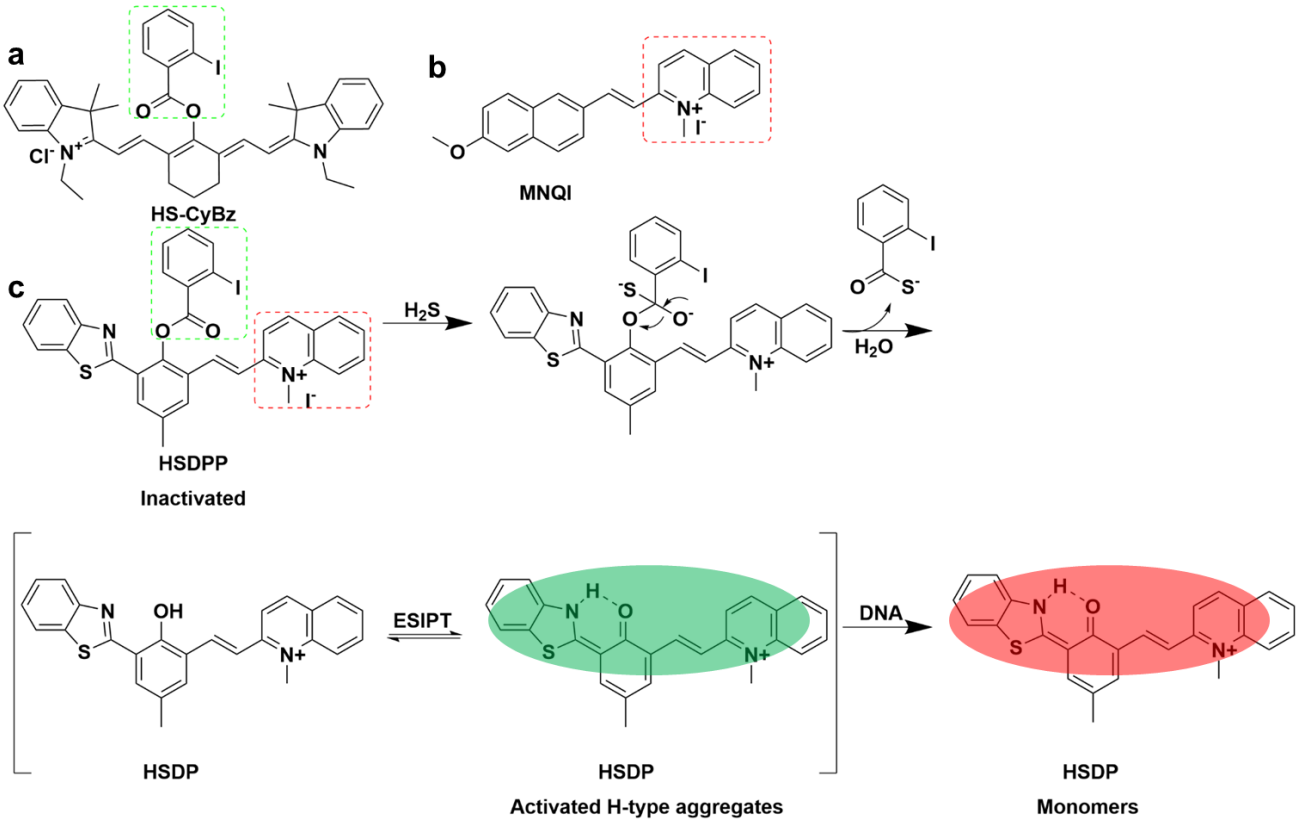

Scheme 1. The design strategy and sensing mode of **HSDPP** in this work. a) The previous work of probe **HS-CyBz** for detecting H_2S; b) The previous work of probe **MNQI** for interacting with DNA. c) The structure and sensing mode of **HSDPP**.

group from **HS-CyBz** (which seemed more selective with smaller steric hindrance) and the binding group from **MNQI** (which interacted with mtDNA), **HSDPP** was designed to achieve the step-by-step detecting system. When initially activated by H_2S, **HSDPP** presented strong green fluorescence via the generation of **HSDP** and H-type aggregates. Subsequently, the interaction between **HSDP** and mtDNA resulted in the confirmation of monomers, which switched the fluorescent signal into the red channel with a practical intensity. Therefore, this strategy could efficiently avoid the interference from spectral overlap, and effectively trace endogenous H_2S upregulation promoted by cystathionase activator SAM in mice brains for

the first time. More than introducing a novel activatable implement, this work brought a mtDNA-regulated switching strategy for transferring fluorescent signals into NIR region, which opened a new window for developing model-specific reporters as well as revealing the crosstalk between target molecules and mtDNA in physiological and pathological prodecures.

Results and Discussion

Design and Recognition Mechanism Studies. In **HSDPP**, iodobenzoic acid methyl ester was selected as the reaction site due to its high selectivity and sensitivity towards H_2S,[40] as shown in Scheme 1a. For mtDNA, the cationic quinolinium group was served as the part of binding unit,[44] which could be also anchored in the mitochondrial (Scheme 1b). In addition, the quinolinium unit could contribute to the aggregation-induced-emission (AIE) feature of the nanoaggregates to some extent.[8] As for the fluorophore, 2-(2-hydroxy-phenyl) benzothiazole (HBT), a universal platform, served as the scaffold ascribed to its unique properties (Scheme 1c). It included advantages such as large Stokes shift, environmental sensitivity and potential for ratiometric sensing.[45] The molecular probe **HSDPP** was synthesized according to the route shown in Supporting Information (Scheme S**1**). The ^{1}H NMR, ^{13}C NMR and mass spectrometry (MS) of **HSDPP**, the activated probe **HSDP** and intermediates were characterized in Figures S1-S12.

The proposed sensing mechanism of **HSDPP** for sequentially visualizing H_2S and mtDNA was shown in Scheme 1c. We hypothesized that the free probe initially exhibited weak fluorescence due to the prevention from the excited-state intramolecular proton-transfer (ESIPT) process by ester. However, the nucleophilic substitution on ester by H_2S would release the hydroxyl group of HBT to induce ESIPT, lead to the formation of the H-type aggregates (the activated probe **HSDP**) and lighted up the platform, accompanied by a shorter emission wavelength; subsequently, **HSDP** would bind to mtDNA to form monomers, which resulted in a bathochromic shift with far red fluorescence emission. Therefore, this nanoprobe could realize the detection of H_2S regulated by mtDNA in biological applications, with multi-channel fluorescent signals.

Spectroscopic Analysis of Probe HSDPP towards H_2S and Mitochondrial DNA. With the probe **HSDPP** on hand, the spectral properties of **HSDPP** in the absence or presence of H_2S (Na_2S as the donor) and mtDNA (calf thymus DNA (ctDNA) as a model) were

10.1002/asia.202000964

determined. As expected, the inactivated probe **HSDPP** (10 μM) alone presented very weak fluorescence and absorbance (Figure 1a and 1b). However, the addition of 200 μM H_2S to the solution of **HSDPP** produced a strong green fluorescence with a peak at 550 nm when excited at 443 nm (Figure 1d), and the equilibrium was reached within 55 min with a 35-fold fluorescence enhancement (Figures 1a, 1c, 1d and S13). At the same time, a remarkable absorbance band at 628 nm was observed (Figure 1b). Moreover, a concentration-dependent fluorescent enhancement could be obtained from 0 to 220 μM H_2S treatment (Figures 1c and S13), and the detection limit was calculated to as 0.124 μM (Figures S14). At this stage, no deep-red signal was obtained (Figure 1a). Further, upon the addition of ctDNA to the above solution, only a slight green fluorescence enhancement could be observed, while the absorption spectrum displayed negligible changes (Figures 1a and 1b). This results suggested that ctDNA itself could not trigger on **HSDPP** fluorescence and the green emission enhancement was caused by H_2S alone.

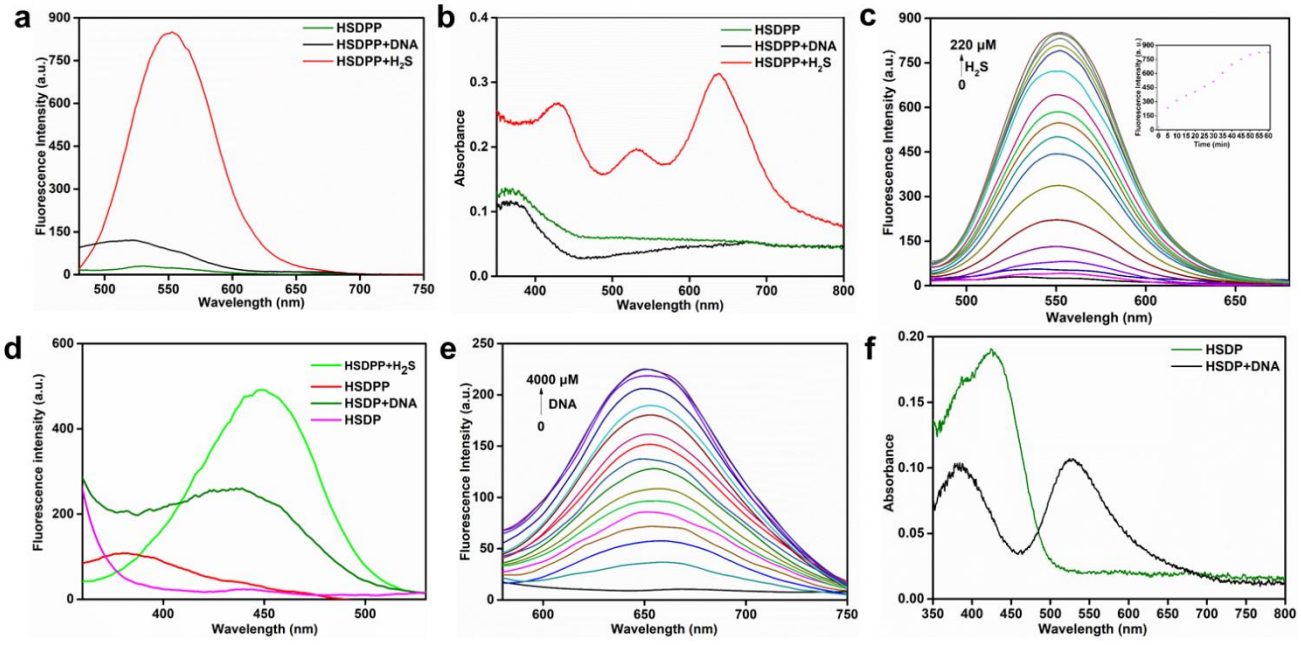

Figure. 1 Response of **HSDPP** towards H_2S and HSDP towards ctDNA, respectively. a) Fluorescence emission spectra of **HSDPP** (10 μM) in the presence or presence of ctDNA (3500 μM)/H_2S (200 μM); b) The absorption spectra of **HSDPP** (10 μM) in the absence or presence of ctDNA (3500 μM)/H_2S (200 μM); c) Fluorescence emission spectra of **HSDPP** after treatment with H_2S for different incubation concentration (0–220 μM). Inset: Time-dependent changes in the fluorescence intensity of **HSDPP** at 550 nm; d) Fluorescence excitation spectra of **HSDPP** (10 μM) in the presence or presence of H_2S (200 μM) and **HSDP** in the presence or presence of ctDNA (3500 μM); e)

Fluorescence emission spectra of **HSDP** after treatment with ctDNA for different incubation concentration (0–4000 μM); f) The absorption spectra of **HSDP** in the absence or presence of ctDNA (3500 μM). All data were acquired in phosphate-buffered saline (PBS) buffer (10 mM, pH 7.4, 1% DMSO) at 37 °C with excitation at 443 nm, the data represent the average of three independent experiments.

However, addition of ctDNA (3.5 M) to the solution of activated probe **HSDP** (10 μM) to form monomers yielded more than 10-fold fluorescence enhancement after being excited at 443 nm (Figure 1d), and the absorbance band at 530 nm was dramatically generated (Figures 1e, S15 and 1f). These results confirmed that **HSDPP** only banded to ctDNA after activated by H_2S.

Isothermal titration calorimetry (ITC) assay showed that the binding constant K_D was 3.03×10^{-5} mol^{-1} and the mtDNA/**HSDP** stoichiometry was 2:1 (Figure S16). In addition, the quantum yield (φ) of **HSDP** and **HSDPP** were 0.0372 (reference: methylene blue (MB)) and 0.00197 (reference: rhodamine B), separately. Furthermore, the detecting system had a large signal resolution of 100 nm between the fluorescence peaks of H_2S and ctDNA responses, which reduced the mutual interference between the two fluorescent peaks and the occurrence of cross-color during cell imaging. Thus, based on this desirable results, the nanoprobe **HSDPP** indicated great potential for visualizing H_2S through the regulating by mtDNA in live cells and *in vivo* with different imaging channels.

To confirm the sensing mechanism, the products of **HSDPP** reacted with H_2S were further confirmed by Electrospray ionization mass spectrometry (ESI-MS) and Ultra performance liquid chromatography coupled with mass spectrometry (UPLC/Triple TOF-MS/MS) (Figure S17 and S18).

AIE feature of activated probe HSDP. To confirm the AIE feature of the activated probe **HSDP**, we initially conducted the spectral experiment of **HSDP** in organic solvent (i.e., dimethyl sulfoxide (DMSO)) with different water content. For the absorption spectra, with the increase of water content, the blue-shifted absorption peak at about 650 nm gradually decreased (Figure S19a). This phenomenon reflected a typical formation of H-type aggregation.[46,47] As for the fluorescence spectra, a certain aggregation-induced quenching phenomenon was also observed, which further indicated that the increase of water content

10.1002/asia.202000964

would cause the aggregation (Figure S19b). Next, in order to ensure whether the aggregation of **HSDP** formed nanoparticles in aqueous solution, dynamic light scattering (DLS) and transmission electron microscope (TEM) experiments were performed. Evidently, the sizes of the aggregates formed by **HSDP** were confirmed to be about 140−190 nm by TEM, while their spherical morphology was also apparently observed (Figure **2**a). Besides, DLS results clearly showed that the aggregates displayed a uniform particle size distribution in Figure **2**b. However, no aggregates about 140-190 nm was found when ctDNA (3500 μM) was added to the solution of **HSDP** by TEM and DLS (Figure S20). Those results indicated that the aggregates could bond to mtDNA to form monomers in solutions.

Selectivity and Stability of probe HSDPP. To investigate the selectivity and anti-interference ability of **HSDPP** towards H_2S, the fluorescence changes of **HSDPP** were also observed in the presence of various relevant species (Figures. 3a and 3b). We found that the strongest response was only towards H_2S, while negligible emission changes were found for other relevant reactive thiols and bio-molecules. This results indicating that the probe was a highly selective sensor for H_2S.

To test the response of this nanoprobe under physiological conditions, the probe was exposed in different pH buffers from 3.0 to 12.0. Accordingly, a relatively wide range of pH applications was observed (Figure S21). Therefore, those results implied that **HSDPP** could be only activated by H_2S in living systems and was stable in mitochondria which possess a weakly alkaline environment.

Imaging exogenous and endogenous H_2S in living HeLa cells. Before cell imaging applications, the colorimetric methyl thiazolyl tetrazolium (MTT) assay was conducted to study

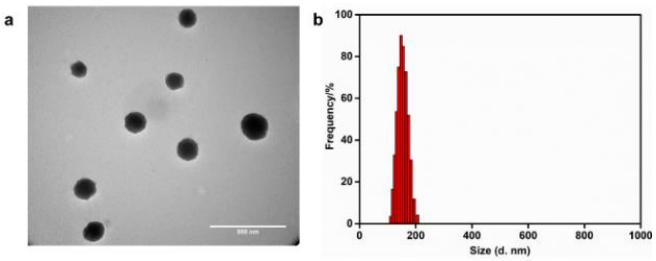

Figure. 2 a) TEM image of **HSDP** in aqueous solution. b) DLS determination for hydrodynamic diameter of **HSDP** in aqueous solution. The scale bar is 500 nm.

the cytotoxicity of **HSDPP** on HeLa cells. As shown in Figure S22, treatment with 0.5–6.0 μM **HSDPP** for 9 h, 12 h and 24 h respectively brought negligible toxicity to living cells, as the cell viability was all above 80%. Thus, the working condition of 5 μM **HSDPP** in 1 h was safe for physiological applications. We then applied this nanoprobe to monitor exogenous and

10.1002/asia.202000964

endogenous H_2S in HeLa cells (Figure 4). It was reported that exogenous Cys could stimulate cells to produce endogenous H_2S in HeLa cells.[48] As we expected, the green and red fluorescence in group c was more obvious, compared with the control group a and b, which implied that **HSDPP** could be used to image endogenous and basal H_2S in HeLa cells. On the contrary, *N*-ethylmaleimide (NEM) was incubated with HeLa cells to investigate that the nanoprobe **HSDPP** could selectively detect H_2S in living cells.[49] Interestingly, the deep-red signal was distinctly decreased and the green channel presented a slight decreased (Figures d1-d4). This could be ascribed to the reduction of the aggregate-type **HSDP** resulted from the inhibition of H_2S production by NEM, which suppressed the transformation of aggregates to the monomers. Thus, the meaningful changing process of different **HSDP** types was visualized in living cells (Figure f). Finally, group **e** indicated that the nanoprobe was also able to detect exogenous H_2S in HeLa cells. As a whole, these above results suggested that **HSDPP** was capable of tracking basal H_2S regulated by mtDNA and monitoring the changes of H_2S levels in live cells. The photostability of **HSDPP** was also examined in HeLa cells, suggesting excellent stability of fluorescence and good performance for long-term traceability in living cells (Figure S23).

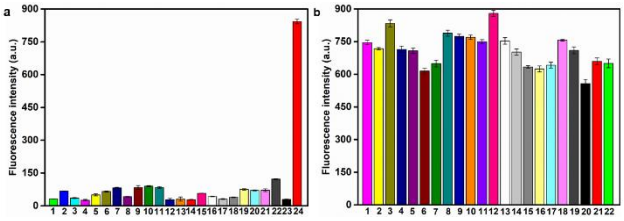

Figure. 3 Probe **HSDPP** (10 μM) with different analytes. a) Probe **HSDPP** (10 μM) with different single analytes. b) Probe **HSDPP** (10 μM) responds to 200 μM H_2S in the presence of various analytes, respectively. (1) CH_3COO^- (2) SCN^-, (3) NO_3^-, (4) NO_2^-, (5) $H_2PO_4^-$, (6) SO_4^{2-}, (7) SO_3^{2-}, (8) $S_2O_3^{2-}$, (9) S_2^{2-}, (10) S_4^{2-}, (11) CO_3^{2-}, (12) K^+, (13) Ca^{2+}, (14) Na^+, (15) Mg^{2+} , (16) Hcy, (17) GSH, (18) Cys, (19) Ser, (20) Leu, (21) H_2O_2, (22) ClO^-, (23) Blank, (24) H_2S. Concentration: 1 mM for Hcy, GSH and Cys. 200 μM for other analytes. All data represent the fluorescence intensities at 550 nm. Data represent the mean ± S.D. of three independent experiments.

Fluorescence Co-localization Experiments. To investigate the subcellular distribution of **HSDPP**, the HeLa cells pretreated with Cys were co-stained with **HSDPP** and different commercial organelle-targeting agents (Figures **5,** S24 and S25). As we expected, the fluorescence of **HSDPP** in green and red channel overlapped better with that of Mito-Tracker Blue in blue channel (Pearson's coefficients were

10.1002/asia.202000964

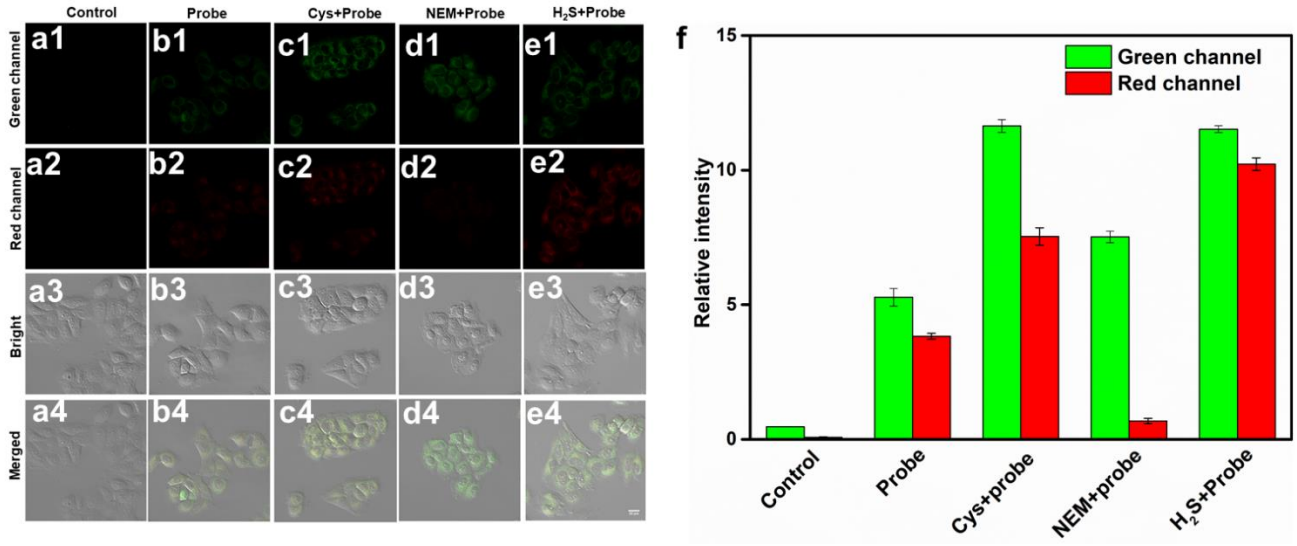

Figure. 4 Cell imaging of probe **HSDPP** (5 μM). a) Control cells. b) Cells incubated with HSDPP for 60 min; c) Cells incubated with Cys (1 mM) and then **HSDPP**; d) Cells incubated with H_2S (200 μM) and then **HSDPP**; e) Cells incubated with NEM (1 mM) and then **HSDPP**; f) The relative fluorescence intensity of group a-f. All confocal imaging was taken after 30 min of pre-processing; λex: 458 nm; Green channel: 400-500 nm; Red channel: 500-600 nm. The scale bar is 20 μm.

0.88449 and 0.0.72067, respectively) than with that of lysosome and nucleus (Pearson's coefficient were 0.66008/0.65479 and -0.17363/-0.11819). In addition, the spatial distribution of the blue, green and red channels in HeLa cells also tended to be consistent (Figure. 5**b**). The results suggested that **HSDPP** had good cell-membrane permeability, and it was an excellent fluorescent tool for accurately displaying H_2S levels and anchoring in the mitochondrial apparatus of cells.

Imaging upregulation of H_2S in mice brains. The activated probe **HSDP** binding to mtDNA afforded a deep-red fluorescence emission (λ_{em} = 650 nm) in the near−infrared (NIR) window, thus it improved contrast and depth of tissue imaging.[50] Importantly, the log P values of **HSDP** and **HSDPP** were 1.270 and 1.269 separately in octanol/water system, which implied the potential **HSDP** and **HSDPP** for effectively crossing the blood–brain barrier (BBB) to achieve imaging in the brain region with the brain-targeted characteristic. Therefore, we assessed **HSDPP** as a NIR imaging probe for tracking the endogenous H_2S upregulation "regulated" by mtDNA in mice brains. The mice were performed direct intraperitoneal (*i. p.*) injection of 0 SAM (200 μL, 100 mg/kg) or saline (200 μL) for 12 h, followed by intravenous (*i.v.*) injection of **HSDPP** (100 μL, 10 μmol/L).

10.1002/asia.202000964

The *in vivo* and *ex vivo* fluorescence images of mice brains were obtained about 1 h later with an IVIS imaging system (Figures 6 and S26). We observed an obvious increase of fluorescence in

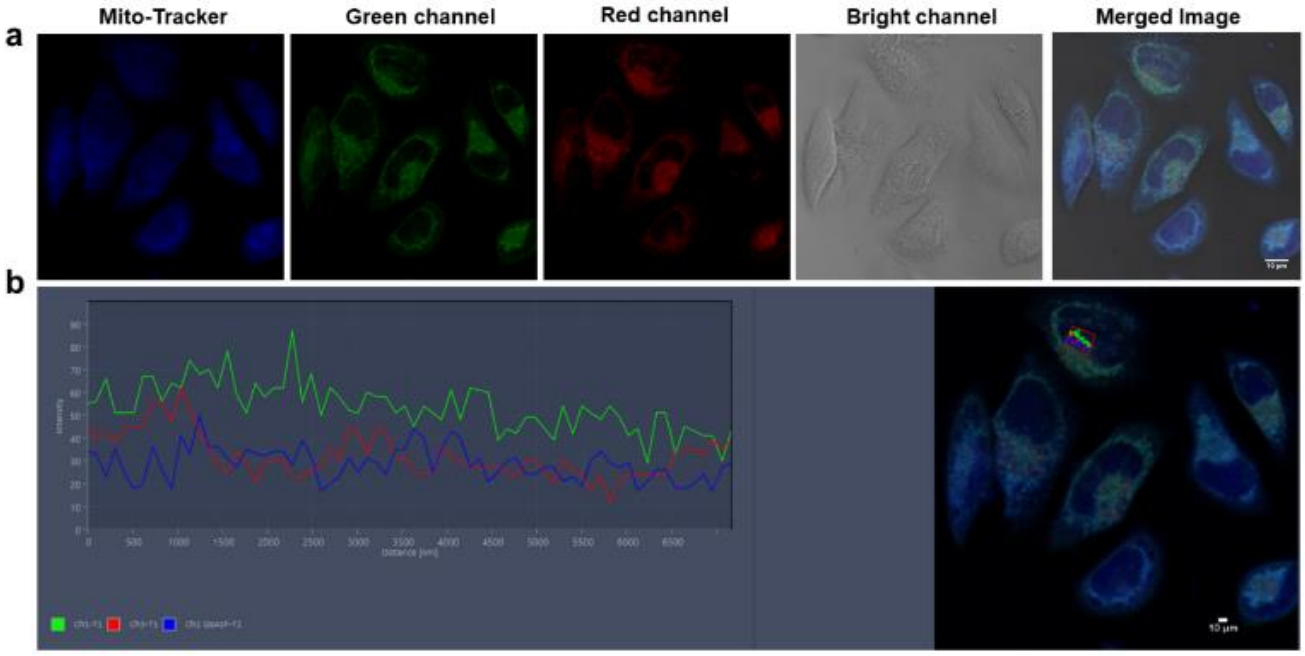

Figure. 5 Fluorescence co-localization experiment. a) Mito-Tracker (MitoLite^{TM} Blue FX490) and **HSDPP**; b) Lift: Intensity profile of linear region of interest across in the HeLa cells co-stained with Mito-Tracker and HSDPP. Right: Hela cells co-stained with Mito-Tracker and **HSDPP**. Mitochondrial dye, λex: 405 nm; λem: 440-500 nm. **HSDPP**, λex: 458 nm; Green channel: 500-600 nm; Red channel: 600-700 nm. The scale bar is 10 μm.

SAM-induced mice brains compared to with that of the saline treated mice. These data demonstrated the capability of **HSDPP** in BBB penetration and tracing the dynamic changes of H_2S levels as well as visualizing the short emssion was "switched" by mtDNA into red signals in the mice brains.

Conclusion

In conclusion, we proposed a novel design method towards the first activatable and switchable probe (**HSDPP**) for monitoring H_2S and tracking the endogenous H_2S upregulation within mitochondrial *in vitro*/*vivo,* with multiresponse signals. In particular, it deserved to be mentioned that, for the first time, we successfully applied this probe for monitoring H_2S "switched" by mtDNA in living cells and mapping the endogenous H_2S upregulation in mice brains. In mechanism, as long as the analytes reacted with the responsive group and induced the process of H-type aggregates changing to monomers, the activatable and switchable probe could realize the consecutive fluorescence imaging. Therefore, our work not

only provides a robust chemical tool for probing endogenous H_2S upregulation *in vitro*/*in vivo*, but also affords a forward-looking design strategy for developing promising versatile or switchable chemosensors for unveiling the interrelated roles of biomolecules and mtDNA in various physiological and pathological conditions.

Acknowledgements

The authors gratefully acknowledge the financial support from the Major Science and Technology Program for Water Pollution Control and Treatment, China (No. 2017ZX07602-002).

Conflict of interest

The authors declare no competing financial interest.

Key words: Activatable and switchable nanoaggregate probe; Hydrogen sulfide; mtDNA; Mice brains.

References

[1] H. Kobayashi, P. L. Choyke, *Acc. Chem. Res.* **2011**, *44*, 83–90.

[2] Y. Lyu, K. Pu, *Adv. Sci.* **2017**, *4*, 1600481.

[3] S. Lee, X. Chen, *Mol. Imaging Probes Cancer Res.* **2012**, 519–543.

[4] M. Swierczewska, S. Lee, X. Chen, *Phys. Chem. Chem. Phys.* **2011**, *13*, 9929–9941.

[5] J. Rao, A. Dragulescu-Andrasi, H. Yao, *Curr. Opin. Biotechnol.* **2007**, *18*, 17–25.

[6] S. Lee, K. Park, K. Kim, K. Choi, I. C. Kwon, *Chem. Commun.* **2008**, 4250–4260.

[7] H. Kobayashi, M. Ogawa, R. Alford, P. L. Choyke, Y. Urano, *Chem. Rev.* **2010**, *110*, 2620–2640.

[8] Z. Guo, C. Yan, W. Zhu, *Angew. Chemie Int. Ed.* **2020**, *59*, 9812–9825.

[9] Y. Lei, W. Ren, C. K. Wang, R. R. Tao, H. J. Xiang, L. L. Feng, Y. P. Gao, Q. Jiang, X. Li, Y. Hu, F. Han, *Theranostics* **2019**, *9*, 5672–5680.

[10] Z. Thiel, P. Rivera-Fuentes, *Angew. Chemie - Int. Ed.* **2019**, *58*, 11474–11478.

[11] J. Cheng, Y. Ren, Y. Huang, X. Li, M. Huang, F. Han, X. Liang, X. Li, *Anal. Chem.* **2020**, *92*, 1409–1415.

[12] L. He, X. Yang, K. Xu, X. Kong, W. Lin, *Chem. Sci.* **2017**, *8*, 6257–6265.

[13] C. Szabõ, *Nat. Rev. Drug Discov.* **2007**, *6*, 917–935.

[14] G. Yang, L. Wu, B. Jiang, W. Yang, J. Qi, K. Cao, Q. Meng, A. K. Mustafa, W. Mu, S. Zhang, S. H. Snyder, R. Wang, *Science (80-.).* **2008**, *322*, 587–590.

[15] F. Yu, P. Li, P. Song, B. Wang, J. Zhao, K. Han, *Chem. Commun.* **2012**, *48*, 2852–2854.

[16] X. Zhang, W. Qu, H. Liu, Y. Ma, L. Wang, Q. Sun, F. Yu, *Anal. Chim. Acta* **2020**, *1109*, 37–43.

[17] F. Yu, X. Han, L. Chen, *Chem. Commun.* **2014**, *50*, 12234–12249.

[18] M. R. Filipovic, J. Zivanovic, B. Alvarez, R. Banerjee, *Chem. Rev.* **2018**, *118*, 1253–1337.

[19] W. Chen, S. Xu, J. J. Day, D. Wang, M. Xian, *Angew. Chemie - Int. Ed.* **2017**, *56*, 16611–16615.

[20] V. S. Lin, W. Chen, M. Xian, C. J. Chang, *Chem. Soc. Rev.* **2015**, *44*, 4596–4618.

[21] Y. Luo, C. Zhu, D. Du, Y. Lin, *Anal. Chim. Acta* **2019**, *1061*, 1–12.

[22] F. Li, Y. Zhou, H. Yin, S. Ai, *Biosens. Bioelectron.* **2020**, *166*, 112476.

[23] J. Mei, Y. Hong, J. W. Y. Lam, A. Qin, Y. Tang, B. Z. Tang, *Adv. Mater.* **2014**, *26*, 5429–5479.

[24] C. Chen, Z. Song, X. Zheng, Z. He, B. Liu, X. Huang, D. Kong, D. Ding, B. Z. Tang, *Chem. Sci.* **2017**, *8*, 2191–2198.

[25] Z. Zou, X. Liao, L. Yang, Z. Huang, H. Yang, Q. Yan, Y. Zhang, Z. Qing, L. Zhang, F. Feng, R. Yang, *Anal. Chem.* **2020**, *92*, 3555–3562.

[26] L. Yang, J. Zheng, Z. Zou, H. Cai, P. Qi, Z. Qing, Q. Yan, L. Qiu, W. Tan, R. Yang, *Chem. Commun.* **2020**, *56*, 1843–1846.

[27] Y. Zhang, S. Yuan, G. Day, X. Wang, X. Yang, H. C. Zhou, *Coord. Chem. Rev.* **2018**, *354*, 28–45.

[28] J. M. Estrela, A. Ortega, E. Obrador, *Glutathione in Cancer Biology and Therapy*, **2006**.

[29] W. Z. Mehal, I. Inayat, R. A. Flavell, *Science (80-.).* **2006**, 847–851.

[30] J. L. Wallace, R. Wang, *Nat. Rev. Drug Discov.* **2015**, *14*, 329–345.

[31] G. C. Kujoth, *Science (80-.).* **2005**, *309*, 481–484.

[32] S. DiMauro, E. A. Schon, *N. Engl. J. Med.* **2003**, *348*, 2656–2668.

[33] S. V Baudouin, D. Saunders, W. Tiangyou, J. L. Elson, J. Poynter, A. Pyle, S. Keers, D. M. Turnbull, N. Howell, P. F. Chinnery, *Lancet* **2005**, *366*, 2118–2121.

[34] A. Latorre-Pellicer, R. Moreno-Loshuertos, A. V. Lechuga-Vieco, F. Sánchez-Cabo, C. Torroja, R. Acín-Pérez, E. Calvo, E. Aix, A. González-

Guerra, A. Logan, M. L. Bernad-Miana, E. Romanos, R. Cruz, S. Cogliati, B. Sobrino, Á. Carracedo, A. Pérez-Martos, P. Fernández-Silva, J. Ruíz-Cabello, M. P. Murphy, I. Flores, J. Vázquez, J. A. Enríquez, *Nature* **2016**, *535*, 561–565.

[35] K. Shimada, T. R. Crother, J. Karlin, J. Dagvadorj, N. Chiba, S. Chen, V. K. Ramanujan, A. J. Wolf, L. Vergnes, D. M. Ojcius, A. Rentsendorj, M. Vargas, C. Guerrero, Y. Wang, K. A. Fitzgerald, D. M. Underhill, T. Town, M. Arditi, *Immunity* **2012**, *36*, 401–414.

[36] A. P. West, G. S. Shadel, *Nat. Rev. Immunol.* **2017**, *17*, 363–375.

[37] R. H. Swerdlow, S. M. Khan, *Med. Hypotheses* **2004**, *63*, 8–20.

[38] R. H. Swerdlow, J. M. Burns, S. M. Khan, *J. Alzheimer's Dis.* **2010**, *20*, DOI 10.3233/JAD-2010-100339.

[39] R. K. Chaturvedi, M. F. Beal, *Free Radic. Biol. Med.* **2013**, *63*, 1–29.

[40] Z. Chen, X. Mu, Z. Han, S. Yang, C. Zhang, Z. Guo, Y. Bai, W. He, *J. Am. Chem. Soc.* **2019**, jacs.9b09181.

[41] C. J. Reinhardt, E. Y. Zhou, M. D. Jorgensen, G. Partipilo, J. Chan, *J. Am. Chem. Soc.* **2018**, *140*, 1011–1018.

[42] Y. Liu, J. Nie, J. Niu, W. Wang, W. Lin, *J. Mater. Chem. B* **2018**, *6*, 1973–1983.

[43] X. Zou, Y. Shi, R. Zhu, J. Han, S. Han, *Anal. Chem.* **2019**, *91*, 15899–15907.

[44] M. Tian, J. Sun, B. Dong, W. Lin, *Angew. Chemie - Int. Ed.* **2018**, *57*, 16506–16510.

[45] A. C. Sedgwick, L. Wu, H. H. Han, S. D. Bull, X. P. He, T. D. James, J. L. Sessler, B. Z. Tang, H. Tian, J. Yoon, *Chem. Soc. Rev.* **2018**, *47*, 8842–8880.

[46] H. Fang, S. Yao, Q. Chen, C. Liu, Y. Cai, S. Geng, Y. Bai, Z. Tian, A. L. Zacharias, T. Takebe, Y. Chen, Z. Guo, W. He, J. Diao, *ACS Nano* **2019**, *13*, 14426–14436.

[47] F. Würthner, T. E. Kaiser, C. R. Saha-Möller, *Angew. Chemie - Int. Ed.* **2011**, *50*, 3376–3410.

[48] H. Zhu, C. Liang, X. Cai, H. Zhang, C. Liu, P. Jia, Z. Li, Y. Yu, X. Zhang, W. Sheng, B. Zhu, *Anal. Chem.* **2020**, acs.analchem.9b04009.

[49] Y. Wang, L. Zhang, S. Zhang, Z. Liu, L. Chen, *Anal. Chem.* **2019**, *91*, 7812–7818.

[50] J. Bin Li, H. W. Liu, T. Fu, R. Wang, X. B. Zhang, W. Tan, *Trends Chem.* **2019**, *1*, 224–234.

10.1002/asia.202000964

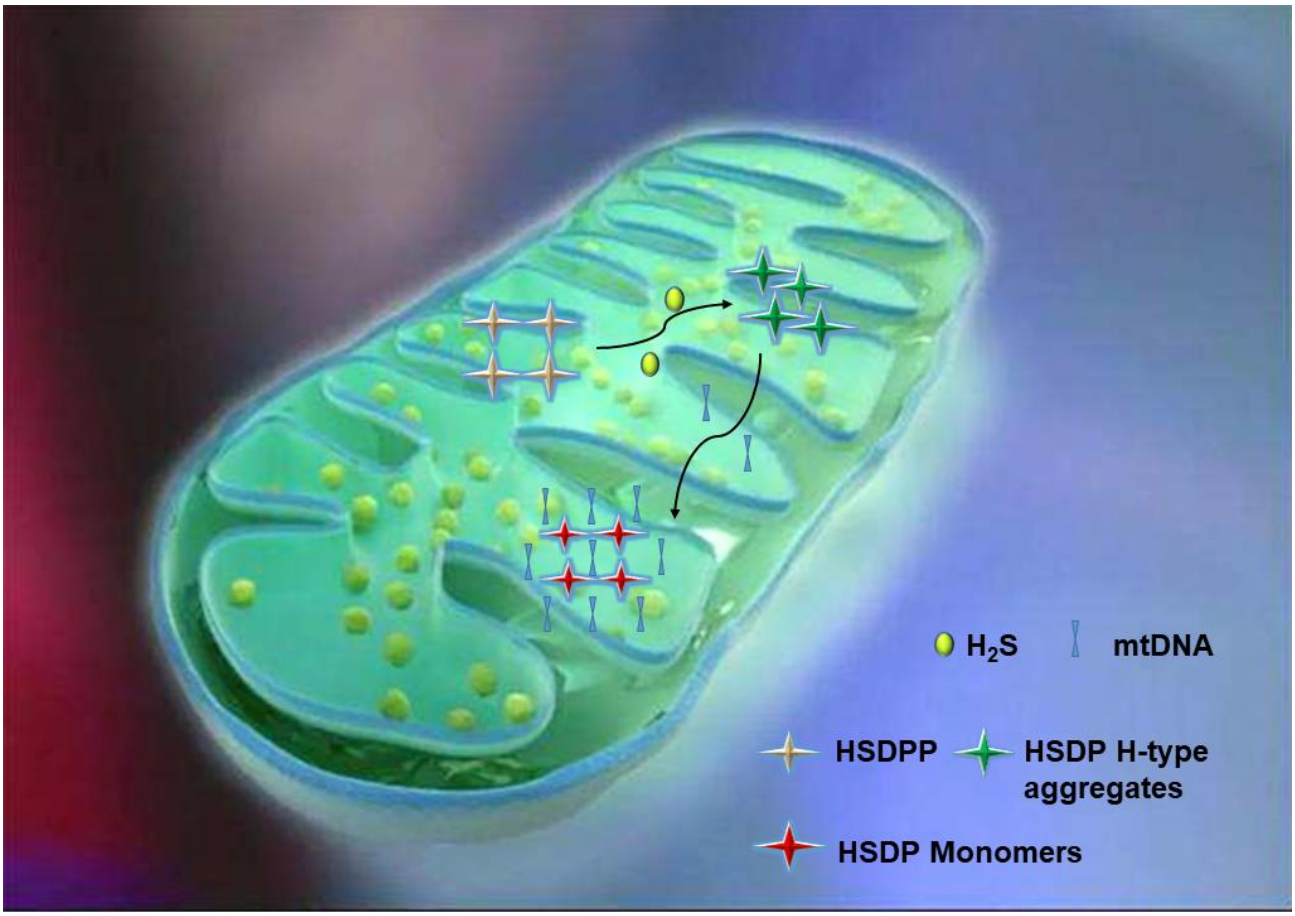

A novel activatable and switchable nanoaggregate probe for detecting H_2S in mice brains was developed. It could be effectively activated by H_2S to form H-type aggregates with green emission; subsequently, the aggregates could bind to mtDNA to form monomers and the emssion color switched from green to deep-red.